Electron Cyclotron Heating in Weakly Relativistic, Finite-Beta Tandem Mirror Plasmas

K. Audenaerde and J. Scharer

March 1982

UWFDM-459

FUSION TECHNOLOGY INSTITUTE

UNIVERSITY OF WISCONSIN

MADISON WISCONSIN

Electron Cyclotron Heating in Weakly Relativistic, Finite-Beta Tandem Mirror Plasmas

K. Audenaerde and J. Scharer

Fusion Technology Institute
University of Wisconsin
1500 Engineering Drive
Madison, WI 53706

http://fti.neep.wisc.edu

March 1982

UWFDM-459

ELECTRON CYCLOTRON HEATING IN WEAKLY RELATIVISTIC, FINITE-BETA TANDEM MIRROR PLASMAS

K. Audenaerde and J.E. Scharer

Fusion Engineering Program

University of Wisconsin

Madison, Wisconsin 53706

March 1982

UWFDM-459

Accepted by Nuclear Technology/Fusion

Abstract

We briefly review ECRF wave and absorption theory and ray tracing and present a numerical model for the study of electron heating in tandem mirror plugs and barriers. It is found that substantial shifts in the spatial energy deposition profile occur from the cold plasma electron cyclotron resonance at elevated temperatures and that surface absorption can be substantial. The O-mode exhibits a ray trajectory which more easily penetrates to the plasma core and has an adequate single pass absorption at temperatures above 10 keV.

1. Introduction

We have formulated a numerical model to study wave propagation and absorption in thermonuclear plasmas in the electron cyclotron resonance frequency range and applied it to investigate the prospects of electron cyclotron resonance heating (ECRH) in mirror devices. This paper aims at reporting these results in a self-consistent way and for this purpose introductory sections on wave propagation and cold plasma ray tracing have been added. An absorption model, largely based on published work, is discussed in section 4. In section 5 this model is applied to plasma ECRH in general with a strong emphasis on the mirror plasmas while section 6 focuses on three different mirror machines, i.e., TASKA, MFTF-B and TMX. Conclusions are summarized in section 7.

2. Wave Propagation and Propagation Regimes[1,2]

Except in the cases of very low fields and densities (i.e., close to the vacuum limit) a magnetically confined plasma is a dispersive medium. That means that in general a wave will have different values for the phase velocity $\bar{v}_{ph} = \frac{\omega}{k^2}\bar{k}$ describing the time evolution of the wave fronts and the group velocity $\bar{v}_{gr} = \frac{\partial\omega}{\partial\bar{k}}$ which accounts for the direction and the speed of the wave energy transport.

From general electromagnetic wave theory applied to the plasma medium, it follows that

$$\bar{n} \times (\bar{n} \times \bar{E}) + \bar{\bar{K}} \cdot \bar{E} = 0 \tag{1}$$

where $\bar{n} = \mathrm{Re}\,\frac{c\bar{k}}{\omega}$ is the refractive index ($n = c/v_{ph}$),

$\bar{E}$ is the wave electric field and

$\bar{\bar{K}}$ is the dielectric tensor which describes the plasma properties. For the simple case of a cold electron plasma at frequencies well above the ion cyclotron frequency

$$\bar{\bar{K}} = \begin{matrix} S & -iD & 0 \\ iD & S & 0 \\ 0 & 0 & P \end{matrix} \tag{2}$$

where $S = \frac{1}{2}(R+L)$ (3)

$D = \frac{1}{2}(R-L)$ (4)

$P = 1-\alpha^2;\ \alpha \equiv \frac{\omega_p}{\omega}$ (5)

$R = 1 - \alpha^2 \frac{\omega}{\omega-\omega_c}$ (6)

$L = 1 - \alpha^2 \frac{\omega}{\omega+\omega_c}$. (7)

Equation (1) can be written in terms of the dispersion tensor $\bar{\bar{D}}$:

$$\bar{\bar{D}} \cdot \bar{E} = 0 \ , \tag{8}$$

which shows that the requirement for a non-trivial solution is the satisfaction of the dispersion relation

$$D \equiv \text{Det} \ (\bar{\bar{D}}) = 0 \ . \tag{9}$$

With θ representing the angle between the confining magnetic field $\bar{B}_0$ and the wave vector $\bar{k}$ the dispersion relation can be reduced to a form introduced by Astrom and Allis:[1]

$$\tan^2\theta = \frac{-P(n^2-R)(n^2-L)}{(Sn^2-RL)(n^2-P)} \ . \tag{10}$$

We will be concerned with arbitrary propagation directions, but it is instructive to show the dispersion relations for propagation perpendicular to the magnetic field ($\theta = \pi/2$):

$$n^2 = \frac{RL}{S} \ ; \quad n^2 = P \ . \tag{11}$$

From this it is obvious that, for certain combinations of parameters, n^2 will go to zero or infinity. The former case is referred to as a cut-off and a ray will usually be reflected in a more or less specular way; the latter is a resonance and strong absorption or emission will occur there. Equations (11) show that cut-offs occur for:

$R = 0$, $L = 0$ affecting the extraordinary mode (wave electric field vector perpendicular to magnetic field)

$P = 0$ affecting the ordinary mode (wave electric field vector parallel to magnetic field)

while one has a resonance (affecting the extraordinary mode only) when $S = 0$. The two different modes arise because the cold plasma dispersion relation is a biquadratic equation in n, in general yielding two different solutions for n^2. One will note that for $\omega \to \omega_c$ the factor R in Eq. (11) goes to infinity, but so does S and the refractive index assumes a finite value. The condition $\omega = \omega_c$, therefore, does not describe a resonance in the sense that n^2 diverges, but nevertheless a strong interaction between the wave and the electron plasma occurs and the term "resonance" is commonly used to describe this interaction. Introducing the variable $\beta \equiv \frac{\omega_c}{\omega}$ one can represent the conditions $R = 0$, $P = 0$, $S = 0$ and $R = \infty$ in an (α^2, β^2) plane to obtain a Clemmow-Mullaly-Allis (CMA) diagram for a one-component (i.e., electron) plasma (Fig. 1). The cut-offs and resonances delineate eight different propagation regimes, each characterized by a particular topology of the wave-normal surfaces (polar plots of the phase velocity).

3. Cold Plasma Ray Tracing[3]

One can write the wave electric field as

$$\overline{E}(\overline{r},t) = \mathrm{Re}\ \{\overline{E}_0(\overline{r},t)\ e^{i\psi(\overline{r},t)}\} \qquad (12)$$

where the amplitude $\overline{E}_0$ and the phase function (or eikonal) ψ are slowly varying functions of position and time. The oscillatory character of the exponential factor causes it to vary rapidly with respect to $\overline{E}_0$. The

propagation vector $\overline{k}$ and the frequency ω can then be defined as the spatial rate of change and the negative of the temporal rate of change of the phase, respectively:

$$\overline{k} = \nabla\psi \quad ; \quad \omega = -\frac{\partial\psi}{\partial t} \, . \tag{13}$$

The dispersion relation (Eq. 9), which in its most general form can be written as

$$D(\overline{k},\omega;\overline{r},t) = 0 \, , \tag{14}$$

restricts the possible combination of $\overline{k}$ and ω to the ones that physically represent those modes that can propagate through the plasma. For a collisionless, magnetized plasma the dispersion tensor is Hermitian and, therefore, its eigenvalues are all real which results in a real dispersion relation. In this picture there is no damping: a mode is either evanescent ($n^2 < 0$) for a certain combination of plasma parameters, or it will propagate over an unlimited distance. Cold plasma ray tracing determines the trajectory of such a mode in an inhomogeneous plasma. It will be shown that in most cases of practical importance this technique gives a very good approximation of the actual ray path.

If the dispersion relation for a particular mode is known explicitly in the form

$$\omega = \omega(\overline{k};\overline{r},t) \tag{15}$$

then ω can be used as the Hamiltonian of a "particle" with energy $\hbar\omega$ and momentum $\hbar k$ and the particle's trajectory is described by the Hamiltonian equations:

$$\dot{\bar{r}} = \partial\omega/\partial\bar{k} \tag{16}$$

(the group velocity!), and

$$\dot{\bar{k}} = -\partial\omega/\partial\bar{r} \ . \tag{17}$$

An alternative form of the ray equations can be obtained by substituting Eq. (13) in the dispersion relation (14):

$$D(\nabla\psi, \frac{\partial\psi}{\partial t} ; \bar{r},t) = 0 \ , \tag{18}$$

i.e., a first order partial differential equation for ψ which sometimes is called the eikonal equation. If ψ changes sufficiently slowly in space and time then this equation can be locally linearized at any point with space-time coordinates $(\bar{r},t)$, and the ray trajectory $\bar{r}=\bar{r}(t)$ is the characteristic of the resulting linear partial differential equation:

$$\bar{A}(\bar{r},t) \cdot \nabla\psi + B(\bar{r},t) \frac{\partial\psi}{\partial t}(\bar{r},t) = C(\bar{r},t) \ . \tag{19}$$

The characteristic is then described by

$$\frac{d\bar{r}}{ds} = \bar{A}(\bar{r},t) \ , \ \frac{dt}{ds} = B(\bar{r},t) \tag{20}$$

with suitable initial conditions. Eliminating the parameter s yields

$$\frac{d\bar{r}}{dt} = \frac{\bar{A}(\bar{r},t)}{B(\bar{r},t)} \, . \tag{21}$$

$\bar{A}$ and B are found by realizing that the coefficients of $\nabla\psi$ and $\frac{\partial\psi}{\partial t}$ correspond to the coefficients of $\bar{k}$ and $-\omega$ in the original equation and therefore: $\bar{A}(\bar{r},t) = \partial D/\partial\bar{k}$; $B(\bar{r},t) = -\partial D/\partial\omega$. We find:

$$\frac{d\bar{r}}{dt} = - \frac{\partial D/\partial\bar{k}}{\partial D/\partial\omega} \, , \tag{22}$$

a form which does not require the explicit solution for ω of the dispersion relation. From Eq. (13) one can derive the conservation law

$$\nabla\omega + \frac{\partial\bar{k}}{\partial t} = 0 \tag{23}$$

and hence

$$\frac{\partial\bar{k}}{\partial t} = - \frac{\partial\omega}{\partial\bar{r}} = \frac{\partial D/\partial\bar{r}}{\partial D/\partial\omega} \, . \tag{24}$$

The ray equations (22) and (24) form a convenient basis for a numerical calculation of the ray trajectories and the evolution of the propagation vector. For a cold plasma, the partial derivatives of the dispersion function D can be calculated analytically such that the ray equations reduce to a system of simultaneous ordinary differential equations which can be solved by a variety of numerical techniques, e.g., a Runge-Kutta scheme.

The requirement that both E_0 and ψ [Eq. (12)] be both slowly varying functions of position (we eliminate the time variable, restricting ourselves

from now on to quasi-stationary plasmas) means that $|\nabla\psi/\psi|^{-1} = 1/|k|$ has to be small compared to the scale length L for variations in the plasma equilibrium. A sufficient condition for this is that the wavelength be small compared to L and that the absorption be weak, i.e., the characteristic absorption distance be large compared to the wavelength. An ordering of the type $L >> k_i^{-1} >> \lambda$ should be possible where k_i is the spatial damping decrement.

In a finite temperature plasma the dispersion tensor is no longer Hermitian. In the usual formulations of geometrical optics (like the one presented earlier in this section) it is assumed that the magnitude of the anti-Hermitian part is much smaller than that of the Hermitian part, but close to the cyclotron resonance this condition can be violated. Weitzner and Batchelor[4] have shown, however, that as long as the wave is weakly damped, ray trajectories can be defined and traced through resonance using the cold plasma dispersion relation.

For this reason it is not necessary to solve the warm plasma ray tracing problem if one has in mind its application to ECRH of a typical fusion plasma. At low temperatures absorption occurs at or close to the $\omega = \omega_c$ surface. Then, however, the absorption coefficient is fairly low, even though the anti-Hermitian part of the dispersion tensor is dominant, and the cold plasma tracing technique will yield correct solutions. At higher temperatures the absorptivity increases strongly, but Doppler and relativistic line broadening move the absorptive area away from the exact cyclotron resonance surface, and the wave is almost totally absorbed before reaching the point where geometrical optics breaks down.

4. Warm Plasma Absorption Around the Electron Cyclotron Frequency

Strong interaction between a wave and the plasma occurs at the cyclotron

frequency $\omega_c = eB/m_e c$ because the wave electromagnetic field oscillates with the frequency at which the electrons gyrate in the confining magnetic field. The cold plasma dispersion relation generally has two roots which means that the plasma can sustain two different propagating modes. If the propagation vector $\bar{k}$ is perpendicular to the confining magnetic field $\bar{B}_0$ then both modes are linearly polarized with respect to the $\bar{B}$-direction and are named extraordinary (X-mode) and ordinary mode (O-mode), depending on whether the wave electric field vector is oriented perpendicular or parallel to $\bar{B}_0$, respectively. As the angle θ included between $\bar{k}$ and $\bar{B}_0$ decreases the polarization becomes elliptic and in the limit where $\bar{B}_0$ and $\bar{k}$ are parallel both modes are circularly polarized with opposite directions for the rotation of the electric field vector. As a rule they have very different phase velocities, and therefore are often labeled as the fast and the slow mode. In CMA-area #7 the slow mode is extraordinary at $\theta = \pi/2$ and right-hand circularly polarized at $\theta = 0$. Because the gyration of the electrons in the confining magnetic field is right-hand circular it can be expected that the slow wave will show a stronger interaction with the plasma electrons than its fast counterpart.

If a propagating wave travels a distance $d\bar{s}$ in a time interval dt, its phase ψ will change by a complex quantity

$$\delta\psi = (\nabla\psi)_{real} \cdot d\bar{s} + \frac{\partial\psi}{\partial t} dt + i(\nabla\psi)_{imag} \cdot d\bar{s} \ . \qquad (25)$$

We allow $\nabla\psi = \bar{k}$ to be complex but restrict $\frac{\partial\psi}{\partial t} = -\omega$ to real values because we are interested in the propagation and possible absorption of stable waves. While the vector character of the real part of $\bar{k}$ describes the normal to the wavefront, the direction of the imaginary part does not have a clear physical

meaning. The vector $\bar{k}_i$ can be defined along any arbitrary direction; we choose $\bar{k}_i \parallel \bar{k}_r$, but other authors have associated it with the direction of the group velocity.

From Eq. (12) it follows that the imaginary part of the expression (25) describes the amplitude attenuation. We can define the power absorption as

$$\alpha \equiv 2k_i \cos \beta \tag{26}$$

i.e., twice the rate of change of ψ_{imag} per unit length, projected on the direction of the group velocity.

At this point one has to generalize the wave dispersion equation to that for a hot plasma. Unless finite temperature effects are taken into account, the dispersion relation is a real equation with solutions for $\frac{ck}{\omega}$ which are either real (i.e. an undamped propagating mode) or purely imaginary (that is, a non-propagating or evanescent mode).

The calculation of the absorption coefficient α has been the subject of extensive research. The theory is mathematically simple for absorption around the harmonics of the electron cyclotron frequency and has been worked out by a number of authors either by solving the finite-temperature dispersion relation[5,6] upon direct evaluation of the emissivity[7] and, recently, from Poynting's theorem.[8] The latter method starts from the stationary energy balance

$$\frac{\omega}{4\pi} \bar{E}^* \cdot \bar{\bar{K}}^A \cdot \bar{E} = \alpha |\bar{S}(\bar{k}_r)| \ , \tag{27}$$

where the left-hand side represents the power absorbed per unit volume in $\bar{k}$-space and $\bar{S}$ is the power flux of which the Poynting flux is the dominant

component; the energy flow of the particles moving coherently in the wave can be neglected for waves in the electron cyclotron frequency range.

Bornatici[9] has shown that for weakly relativistic plasmas near resonance the absorbed power (i.e., the left-hand side of Eq. 27) is given by

$$\frac{\omega}{4\pi}\,\bar{E}^{*}\cdot\bar{\bar{K}}^{A}\cdot\bar{E}=\frac{\omega}{4\pi}\,K_{xx}^{A}\left|E_x-iE_y+\frac{\omega-n\omega_c}{\omega}\,\mathrm{tg}\theta\,E_z\right|^2 \quad . \tag{28}$$

The factor in absolute value brackets describes the effect of wave polarization and attributes variations in power absorption either to changes in the polarization in a plane perpendicular to $\bar{B}_o$ or to the presence of a longitudinal component E_z along $\bar{B}_o$. A solution which is valid for mildly relativistic temperatures is obtained by evaluating K_{xx}^{A} for the hot plasma while using the cold plasma dispersion tensor to find the eigenvector (E_x, E_y, E_z). For oblique propagation one finds eventually

$$\alpha_n^{x,o}(\omega,\theta)=\pi\,\frac{n^{2n-1}}{2^n(n-1)!}\,\frac{\omega_p^2}{c}\,\left(\frac{v_{th}}{c}\right)^{2(n-1)}(\sin\theta)^{2(n-1)}\,(1+\cos^2\theta)$$
$$\times\,\phi_n(\omega,\theta)\left[\frac{N^{2n-3}}{1+\cos^2\theta}\,\frac{|E_x-iE_y|^2}{4\pi|\bar{S}|/cN}\right]_{N=N^{x,o}} \quad . \tag{29}$$

The thermal velocity v_{th} is defined as $(2kT_e/m)^{1/2}$, and $n \geq 2$ is the harmonic number. In this expression $\bar{S}$ still has to be evaluated using the cold plasma eigenvector $\bar{E}$. In Eq. (29) most symbols have their usual meaning; $N = ck_r/\omega$ is the index of refraction, n is the harmonic number and ϕ_n represents the normalized Doppler absorption profile

$$\phi_n(\omega,\theta)=\frac{e^{-\zeta_n^2}}{\sqrt{2\pi}\;\omega N\cos\theta\;\left(\frac{v_{th}}{c}\right)} \tag{30}$$

with $\zeta_n \equiv \frac{1}{\sqrt{2}} \frac{\omega - n\omega_c}{\omega} \frac{c}{v_{th}} \frac{1}{N \cos\theta}$.

For perpendicular propagation, i.e. when $N|\cos\theta| < v_{th}/c$, the absorption coefficient for the extraordinary mode is still adequately described by Eq. (29) if one replaces $\phi_n(\omega,\theta)$ by the normalized relativistic profile function $\bar{\phi}_{n+3/2}(\omega)$:

$$\bar{\phi}_q(\omega) = \frac{1}{\Gamma(q)} \left(\frac{c}{v_{th}}\right)^{2q} \left(\frac{|\omega - n\omega_c|}{\omega}\right)^{q-1} \frac{1}{\omega} e^{-(c^2/v_{th}^2)(|\omega-n\omega_c|/\omega)} \quad . \tag{31}$$

For the ordinary mode at $\theta = \pi/2$ the effect of E_z, i.e. the component of the wave electric field along the confining magnetic field, is dominant in Eq. (28) and the absorption coefficient becomes

$$\alpha_n^o(\omega,\theta=\pi/2) = \pi \frac{n^{2n-1}}{2^n(n-1)!} \frac{\omega_p^2}{c} \left(\frac{v_{th}}{c}\right)^{2(n-1)} (\sin\theta)^{2(n-1)} (1 + \cos^2\theta) \tag{32}$$

$$\times \bar{\phi}_{n+5/2}(\omega) \, (N_\perp^o)^{2n-1} \left(\frac{v_{th}}{c}\right)^2 \quad ,$$

a result which shows clearly that the absorptivity of the ordinary mode will be lower than that of the extraordinary mode by a factor of order $(v_{th}/c)^2$.

At the fundamental frequency the situation is mathematically more complicated because the term $k_\parallel v_\parallel$ in the resonance condition

$$\omega - k_\parallel v_\parallel \pm \omega_c = 0 \ , \tag{33}$$

which is of little importance compared to $(\omega \pm \omega_c)$ as long as $\omega \approx n\omega_c$ with $n > 2$, can no longer be neglected when $n = 1$, and $|\omega - \omega_c|$ is small.

Another complication arises from the fact that $\omega_c \equiv eB/mc$ is energy dependent via the relativistic change of the electron mass. Inspection of Eq.

(33) shows that in the Doppler regime only the longitudinal component of the electron velocity contributes to the fulfillment of the resonance condition, but that the magnitude of the velocity determines the resonance when $\theta \to \pi/2$ and $v_{\parallel}$ vanishes.

At the fundamental frequency the absorption coefficient is most conveniently calculated from the energy balance for the X-mode and in the case of oblique propagation for the O-mode; for perpendicular propagation in the ordinary mode the dispersion tensor is sufficiently simple to allow the determination of Im(k) directly from the dispersion relation.

One eventually finds the following results, valid for moderate values of $(v_{th}/c)^2$ at frequencies in the fundamental electron cyclotron resonance range, ignoring finite Larmor radius effects:

In the relativistic regime (i.e. $v_{th}/c > (ck/\omega)|\cos\theta|$):

ordinary mode:[10]

$$\alpha_1^o = \frac{1}{\sqrt{2}} \sqrt{1 - \frac{\omega_p^2}{\omega^2} \frac{\omega_p^2}{\omega^2}} \frac{\omega}{c} \frac{-F''_{7/2}(z_1)}{|G_{7/2}|\sqrt{G'_{7/2} + |G_{7/2}|}} \tag{34}$$

extraordinary mode:

low density[11]
$$\alpha_1^x = -\frac{1}{2} \frac{\omega_p^2}{\omega^2} \frac{c^2}{v_{th}^2} \frac{\omega}{c} F''_{5/2}(z) \tag{35}$$

high density[10]
$$\alpha_1^x = \sqrt{2}\,(1 - \frac{\omega_p^2}{2\omega^2})^{3/2} \frac{\omega^2}{\omega_p^2} \frac{v_{th}^2}{c^2} \frac{\omega}{c} \frac{-F''_{5/2}(z)}{|F_{5/2}(z)|^2} . \tag{36}$$

In the Doppler regime, i.e. oblique propagation, both modes can be described by the same expression, using appropriate values for the refractive index ck/ω:

low density[12] $$\alpha_1^{x,o} = \frac{\sqrt{\pi}}{2} \frac{\omega_p^2}{\omega^2} \frac{\omega}{c} \left(1 + \frac{c^2k^2}{\omega^2}\right) \frac{c}{v_{th}} \frac{\omega^2}{c^2k^2|\cos\theta|} e^{-\left(\frac{c}{v_{th}} \frac{\omega-\omega_c}{\omega\cos\theta}\right)^2} \quad (37)$$

high density[10] $$\alpha_1^{x,o} = 2\sqrt{2}\, R^{x,o} \frac{v_{th}}{c} \frac{\omega}{c} \mathrm{Im}\left(\frac{-1}{Z(\zeta)}\right) . \quad (38)$$

Here $Z(\zeta)$ is the familiar plasma dispersion function:[13]

$$Z(\zeta) \equiv 2i\, e^{-\xi^2} \int_{-\infty}^{i\xi} e^{-t^2}\, dt \quad ; \quad \zeta = \frac{\omega - \omega_c}{k_\parallel v_{th}} \quad (39)$$

and F_q is the relativistic dispersion function:[5,6]

$$F_q(z) \equiv -i \int_0^\infty \frac{e^{izt}}{(1 - it)^q}\, dt \quad ; \quad z = \frac{c^2}{v_{th}^2} \frac{\omega - \omega_c}{\omega} \quad . \quad (40)$$

R^X and R^O are complicated functions of θ and the ratios ω_p/ω and ω_c/ω.

Plotting the absorption coefficient versus the normalized frequency shows that both the magnitude of the absorptivity and the width of the profile increase rapidly with temperature (Figs. 2a-d). At an electron temperature of 50 keV the line width is of the order of the electron cyclotron frequency itself. This has three important consequences. First, overlap of harmonics is going to play an increasingly important role when temperatures increase. Secondly, depending on the magnitude and direction of ∇B, this wide profile will translate into a very wide absorption layer (of the order of a meter in a typical tandem mirror barrier region). Third - and most difficult to deal with in the design of a heating system - the minimum frequency at which appreciable absorption occurs is a function of temperature.

A peak absorption coefficient of 10 cm^{-1} is a fairly typical value for the slow mode, but it implies that after traveling 1 cm through the plasma only a negligible fraction of the launched power (e^{-10}) will be left.

Absorption will be very strong, but can be localized on the surface of the plasma. A very high absorption coefficient is as undesirable as a very low one, and in many practical cases it will be necessary to choose the frequency - or, conversely, the position of the heating zone - such that the absorption coefficient is in the range of a few tenths per centimeter path length.

5. Electron Cyclotron Resonant Heating

There exists a number of different situations where electron cyclotron heating can be an attractive way of heating a thermonuclear plasma's electron population. In contemporary experiments insufficient heat is produced in the plasma - if any at all - to sustain the desired electron temperature. Direct heating of the electrons can then be contemplated as a supplementary energy source in conjunction with ICRF or neutral beam heating of the ions. Temperatures are typically low enough to allow a slow mode wave to penetrate to the core of the plasma and take advantage of its high absorption coefficient which typically is a factor $(c/v_{th})^2$ larger than that of the fast (or O) mode. Electron cyclotron heating becomes most important in tandem mirrors because of the necessity to keep the plug electrons hot enough to produce the high excess positive potential required to confine the central cell ions. This excess potential is the Φ_c-portion of the total potential difference $\Phi_b + \Phi_c$ (see Fig. 4) which is a nearly linear function of the plug electron temperature T_{ep}:

$$\Phi_b + \Phi_c = T_{ep} \ln \left(\frac{n_p}{n_b - n_{eh}} \sqrt{\frac{T_{ec}}{T_{ep}}}\right) . \tag{41}$$

Here T_{ec} is the central cell electron temperature and n_p, n_b and n_{eh} are the densities of the potentially trapped plug electrons, the total electron population of the barrier and the hot mirror-trapped electrons in the barrier,

respectively. The factor $\sqrt{T_{ec}/T_{ep}}$ accounts for the non-Maxwellian character of the electron distributions.[14] Even if the device achieves ignition in the central cell, direct heating of the barrier electrons would still be required. In an ignited toroidal reactor, on the other hand, there is no need to sustain direct electron heating during the burn phase and a pulsed ECRH system will only be useful during the startup period in combination with ICRH and/or neutral beam injection.

A fundamental difference between electron cyclotron resonance heating in toroidal and linear devices arises from the different geometries (Fig. 3). In a perfectly toroidal magnetic field which falls off with 1/R, the resonance condition $\omega = n\omega_c$ ($n = 1,2,3, \ldots$) is satisfied on a surface in the shape of a right circular cylinder. The heating wave is generally launched in the equatorial plane, either from the inside (X-mode) or the outside (O-mode) of the torus, depending on the mode that has been selected. Therefore, the ray trajectories can intersect the magnetic field lines more or less perpendicularly and the dominant absorption mechanism can be made to be relativistic or Doppler in nature [see Eqs. (34-36)] - depending on which is desired.

In a linear device the resonance condition is generally satisfied on a distorted disc whose location along the z-axis depends on the axial dependence of the magnetic field taking β-effects into consideration. Ideally the strongest absorption should be arranged to occur in the core of the plasma. As a consequence a rather grazing incidence of the heating wave is required and the ray trajectories will intersect the field lines at sufficiently small angles to make the Doppler mechanism dominant unless the plasma has an electron temperature exceeding $\sim$ 100 keV.

The grazing incidence, however, causes an extra complication

characteristic to linear devices that practically restricts the heating wave to the fast mode, i.e., the mode which is left hand circularly polarized in the case of propagation parallel to the magnetic field lines. The index of refraction is equal to the ratio between the speed of light and the phase velocity of the wave and, therefore, is larger than unity for the slow mode. This implies that, in agreement with Snell's law of geometrical optics, a slow wave launched at a grazing angle with respect to the plasma surface will be bent towards the normal to this surface, i.e., away from the resonant layer. Refraction effects are much weaker for a fast wave and, in any case, have the opposite tendency of bending the ray trajectory away from the normal. Propagation will thus be rather parallel to the field line which enhances the dominant Doppler character of the absorption mechanism.

We are now in a position to appreciate the criteria one can use to define an "acceptable" solution to the electron cyclotron resonant heating probem in any given plasma device.

a) The only available power sources in the relevant frequency range of 20-200 GHz are gyrotrons - costly devices that do exist or will exist at selected frequencies and for all practical purposes have a narrow band output spectrum. Research on tunable free-electron lasers operating in this frequency range is still in an early stage. Thus, no variation of the signal frequency can be allowed during the startup phase of the device.

Selection of the wave frequency should take into account this limited availability of wave sources capable of operating at sufficiently high energy levels. While most present-day devices and projected toroidal reactors are either pulsed machines or need ECRH only during the startup phase, a tandem mirror with thermal barriers requires several megawatts of RF power to be delivered in a continuous wave (CW) mode. Gyrotrons capable of delivering

power levels of the order of 250 kW either CW or in long pulses exist or are being developed only at selected frequencies: 28 GHz, corresponding to a 1 tesla confining field, 56/60 GHz and, in an experimental stage, a number of frequencies in the 100-120 GHz range. These are tubes developed by U.S. companies. The Russian program generally aims at somewhat higher frequencies and similar power levels, e.g., the 86 GHz pulsed high power gyrotron in use in the T-10 experiment.

b) Fusion devices are very crowded and consist of a large number of complicated systems. The ECRH launching structure should be compact and oriented in a fixed direction.

c) The transport system between wave source and plasma should have low losses, avoid arcing and show a low susceptibility to neutron damage. Present experiments generally use oversized circular waveguides which are too lossy to be considered for high power CW application in reactor-type devices. Recently, a beam waveguide launcher has been proposed[15,17] which uses an offset Cassegrain system consisting of paraboloidal and hyperboloidal reflectors. Such a system spatially combines the beams of a number of gyrotrons to achieve the required power levels and isolates the gyrotrons from neutron and plasma flux while allowing good vacuum pumping in the intervening region.

d) Penetration of the plasma should be good, i.e., most of the wave energy should be absorbed by the core of the plasma. An excessively high absorption coefficient will cause 100% surface absorption if the plasma appears as a black body at the local electron cyclotron resonance frequency.

e) Absorption should be near 100% for a single pass through the plasma. To a certain extent this criterion is in contradiction to d), and one has to expect a fairly narrow window in parameter space where both

requirements are satisfied - if such a window exists at all.

In the next section we will explore how these considerations lead to quite realistic ECRH systems in tandem mirror reactor and experiment designs.

6. ECRH in Mirror Machines

At the University of Wisconsin a code (ECPUB) has been designed[16] to study the propagation and absorption of electromagnetic waves close to the electron cyclotron resonance frequency of the plasma. It is characterized by the numerical solution of the geometric optics equations (as outlined in section 3) and the integration along the ray trajectory of the plasma absorption coefficient obtained via the warm-plasma theory described in section 4. Magnetic field lines, cut-off and resonance surfaces, and wave vectors are plotted in an attempt to contribute to the physical understanding of the sometimes unexpected ray trajectories and absorption patterns. The data representing the ray trajectories are plotted at fixed time intervals of 10^{-10} s and, therefore, their separation can be used as a measure for the phase velocity. The numbers 1-7 represent the percentage of incident energy absorbed up to the point where they are printed; they stand for 25, 50, 75, 90, 95, 99 and 100% absorption, respectively. We used this code to evaluate the prospects of ECR heating in an existing experiment (TMX), an experiment under construction (MFTF-B) and a reactor design (TASKA).

Figure 4 shows schematically the axial magnetic field and potential profiles of the three machines. The arrows indicate where and at which field strength ECRH will be applied. One notes that only MFTF-B has a thermal barrier, a feature requiring heating at two different locations and thus two different frequencies.

6.1 A Tandem Mirror Reactor Study: TASKA[17]

Here electron cyclotron resonant heating is required to maintain the high

potential in the plug region which in its turn provides for the electrostatic confinement of the central cell ions [cf. Eq. (41)]. Good central cell confinement in TASKA was found to require a plug electron excess potential of 43 keV and this in turn demands a plug electron temperature of ca. 60 keV. The availability of a 56 GHz gyrotron was the main reason in choosing the 2 tesla point as the center of the heating zone. In this particular area the magnetic field is in transition from solenoidal to a yin-yang minimum-B field, and therefore an analytic description is not readily available. While it is possible to couple ECPUB to a callable version of a magnetic field code like EFFI, preference was given to a simple regression model based upon regular EFFI calculations.

The plasma electron density and temperature were assumed not to vary in axial direction over the heating zone (ca. 1 m) and their radial profiles were represented by

$$n_e = n_{eo}\, e^{-(r^2/a^2)^5}$$
$$T_e = T_{eo}\, e^{-(r^2/a^2)^5}, \qquad (42)$$

respectively. For every point along the ray trajectory the β-factor is calculated and the vacuum magnetic field is corrected accordingly. Figs. 5a-d clearly show the deformation and the displacement of the cyclotron resonance surface due to the finite β-effect at higher electron energy densities. The heating system was designed to be as efficient as possible in steady-state operation, i.e., at an electron temperature of about 60 keV. At such a temperature, the slow mode (extraordinary mode in the case of propagation perpendicular to the confining magnetic field) has a number of very

unattractive features. The ray trajectories are bent away from the heating zone, necessitating a grazing incidence at the wave and a launcher which is nearly parallel to the axis of the machine. But there simply is not enough room for such a mounting which would, furthermore, make the structure very vulnerable to neutron damage. The slow mode also has a very high absorption coefficient, and at 60 keV the plasma appears as a blackbody which totally absorbs the wave at the plasma surface. For these reasons the use of waves with X-type polarization was rejected altogether.

The fast mode (ordinary mode in the case of perpendicular propagation) displays little refraction. One expects no severe penetration problems with this mode at the densities and temperatures of the TASKA design. A central electron density of 1.1×10^{13} cm^{-3} puts the local plasma frequency (a cut-off for the fast mode, see section 2) at 29.8 GHz which is well below the electron cyclotron frequency at 56 GHz.

Figure 5a-d shows ray trajectories and absorption levels for various temperatures up to the steady-state value of 60 keV. The launching point is chosen 0.5 m outwards from the 2 tesla-point and the frequency is kept at 56 GHz. At 5 keV absorption of the fast mode is already considerable: the rays with 60°, 55°, and 50° incidence reach 46, 66, and 68 percent absorption, respectively. While this will contribute substantially to the plasma heating in the early startup phase (especially as the reflected wave will eventually be absorbed somewhere in the plasma) it is to be expected that during the early phase additional heating will have to be provided. At 10 keV the corresponding percentages are 68, 88, and 95, while for higher temperatures the absorption can be considered complete for most directions, with the 60° launching direction giving the best penetration.

Careful examination reveals that the absorption is not symmetric about

the cyclotron resonance surface. This is explained by the decrease of the angle θ included between the wave vector and the field lines as the wave progresses along its trajectory, causing a corresponding decrease of the local absorption coefficient.

Concluding, it can be stated that a wave

- launched with ordinary polarization
- at 56 GHz
- at 60° with respect to the normal to the plasma surface

will be totally absorbed by the plasma in the electron temperature range between 10 and 60 keV, while contributing strongly to the plasma heating at the lower temperatures typical for the early startup phase.

6.2 The MFTF-B Experiment[18,19]

In this experiment, presently under construction, electron cyclotron resonance heating again will be used to create the confining potentials at each end of the machine by increasing the plug electron temperature T_{ep} (cf. Eq. 41). Unlike the TASKA design, however, ECRH will also be applied to the thermal barriers.

One of the characteristics of MFTF-B is the use of so-called A-cells to create the electrostatic potential well confining the central cell ions so that the functions of providing MHD-stability and electrostatic confinement are split between the yin-yang and the A-cell, respectively. As pointed out in section 4 [Eq. (41)] the quality of the confinement depends strongly on the electron temperature in the A-cell (plug), and, just as in TASKA, electron cyclotron heating at the 2 tesla point (56 GHz, 350 kW on each side) is planned in MFTF-B.

Thermally insulating the electrons in the yin-yang and the central cell from those in the plug reduces the power loss from the plug and allows for a

considerable reduction of the required ECRH energy. A thermal barrier is built up at the bottom of the magnetic well by applying ECRH from a second set of gyrotrons at the 1 tesla point (28 GHz, 220 kW on each side). The thermal barrier's operation is based on the fact that ECRH preferentially contributes to the perpendicular energy of the electrons and thus captures a fraction of the passing hot electrons in the barrier. This means that n_{eh} in Eq. (42) increases, further contributing to the buildup of the combined potential difference $\phi_b + \phi_c$ which confines the plug electrons.

Figure 6a-d shows typical absorption patterns at a 50 keV electron temperature for heating at the 1 and 2 tesla point, and the ordinary and extraordinary modes. Analytic models are used for the magnetic field and the plasma electron density and temperature. Beta effects are taken into account, and the corresponding deformation of the resonant layer is clearly visible. At both locations we see very strong absorption of the X-mode, and the corresponding severe penetration problem. The ordinary mode on the other hand shows total single-pass absorption and good penetration. Its rays clearly belong to two different groups, one where the Doppler effect is dominant and another - almost perpendicular to the field lines - where the absorption is mainly relativistic.

6.3 An "Overdense" TMX

The TMX device is a simple tandem mirror lacking A-cells or thermal barriers. Magnetohydrodynamic stability is achieved by terminating the machine by a set of yin-yang coils at each end. Electron cyclotron heating could be applied to the yin-yang plug area to heat the magnetically trapped electrons and create a potential peak to confine the central cell ions. This hypothetical case has been studied, increasing the electron density in the yin-yang by about a factor 5 to 5×10^{13} cm^{-3}. The magnetic field was

modelled analytically[20] and the density profile was assumed to follow the flux surfaces, falling off exponentially.

This situation is of particular interest from a theoretical point of view, as the plasma topology is sufficiently complicated to divide a volume with a characteristic linear dimension of less than 50 cm in a large number of areas representing seven of the eight possible CMA regions discussed in section 1. Figure 7 shows the ray trajectories and absorption profiles.

With an electron temperature of 200 eV one has to rely on the extraordinary mode to obtain sufficient absorption. While the absorption coefficient reaches a value of 5 cm^{-1}, for the ray launched at a 30° angle the area over which significant absorption occurs is only 1 cm wide. At the point where $\omega_p = \omega_c$ theory predicts that finite density effects will reduce α to negligible values and the peak value of the absorption is reduced accordingly when a ray approaches that point. The absorption spectrum also becomes wider, however, which results in an weakly absorbing layer a few centimeters thick. For the 15° launching direction, α has become so small (peaking at 0.11 cm^{-1}) that even two passes through the resonance surface don't yield more than 35% absorption. At this low temperature there is no penetration problem, but the plasma topology is such that a slow wave encounters two evanescent areas (CMA areas 2 and 3). Unless the density is kept below, say, 10^{13} cm^{-3} the core of the yin-yang plasma will be inaccessible, even to the extraordinary mode. The low temperature and corresponding low absorption preclude the use of the ordinary mode. For the latter the right-hand cut-off does not represent a barrier, but it would be reflected at the $\omega = \omega_p$ surface - an even less favorable situation.

7. Conclusions

We cannot escape the conclusion that the application of ECRH to create

the high potential peak required in tandem mirror operation is subject to a number of challenges, widely varying for different types of devices and sometimes contradictory. Within the framework of the model presented here (which does not allow for strongly relativistic nor anisotropic electron distributions) it can be concluded that:

a. In a minimum-B geometry evanescent zones can be present limiting the accessibility of the wave to the plasma core.

b. At high temperatures and a fixed frequency resonating near the core the plasma becomes a blackbody causing surface absorption and again preventing access to the center of the plasma. This appears to be by far the most serious problem.

c. As soon as the electron temperature exceeds about 1 keV the absorbing layer becomes quite thick, resulting in absorption long before the wave reaches the resonant surface. This implies that heating at a frequency far below the resonant frequency is possible, allowing for some relief from the problem mentioned under b. In general one should expect that a limited window in parameter space through which efficient ECRH is possible will exist but must be carefully designed to match the confinement properties (magnetic field, density, β and temperature profiles) of the device to be heated. Previous success in the ECRF range suggests that useful solutions to enhance tandem mirror confinement will be found.

Acknowledgement

Many discussions with J. Shearer, D. Batchelor, B. Stallard, J. Beyer, N. Lam and J. Santarius are gratefully acknowledged.

This research was supported by DOE Contract DE-AC02-80ER53104 (Task III) and Research Agreement #130/D2/524350 with the Kernforschungszentrum Karlsruhe.

References

1. Stix, T.H., The Theory of Plasma Waves, New York, 1962.

2. Boyd, T.J.M, and J.J. Sanderson, Plasma Dynamics, New York, 1969.

3. Batchelor, D.B., R.G. Goldfinger and H. Weitzner, IEEE PS-8 (1980) 78.

4. Weitzner, H.R., D.B. Batchelor, Phys. Fluids 23 (1980) 1359.

5. Dnestrovskii, Yu.N., D.P. Kostomarov and N.V. Skrydlov, Zh. Techn. Fiz. 33 (1963) 922. [English translation: Sov. Phys. - Tech. Phys. 8 (1964) 691].

6. Shkarofsky, I.P., Phys. Fluids 9 (1966) 561.

7. Audenaerde, K., Plasma Physics 19 (1977) 299.

8. Bornatici, M., F. Engelmann and V. Petrillo, Xth European Conference on Controlled Fusion and Plasma Physics, Moscow, 1981. Paper H-14.

9. Bornatici, M., VIIIth Annual Conference on Plasma Physics, Swansea, 1981. Invited paper.

10. Bornatici, M., Proceedings of International Workshop on ECE and ECRH, Oxford 1980. Report CLM-ECR (1980).

11. Bornatici, M. and F. Engelmann, Radio Science 14 (1979) 309.

12. Fidone, I., G. Granata, G. Ramponi and R.L. Meyer, Phys. Fluids 21 (1978) 645.

13. Fried, B.D. and S.D. Conte, The Plasma Dispersion Function, New York, 1961.

14. Cohen, R.H., I.B. Bernstein, J.J. Dorning and G. Rowlands, Nucl. Fusion 20 (1980) 1421.

15. Beyer, J., J. Scharer and K. Audenaerde, 9th Symposium on Engineering Problems of Fusion Research, Chicago, 1981. Paper 4Q8.

16. LIBRIS Physics Library, NMFECC Livermore, CA. Code P52.

17. Badger, B., et al., "TASKA, A Tandem Mirror Fusion Engineering Facility", Univ. of Wisconsin, UWFDM-500/FPA-82-1/KfK-3311, March 1982.

18. Baldwin, D.E., B.G. Logan and T.C. Simonen (editors), "Physics Basis for MFTF-B", UCID-18496, 1980.

19. Shearer, J.W. and K. Audenaerde, 23rd Annual Meeting of the Division of Plasma Physics of the APS, New York 1981. Paper 4P20.

20. Kaiser, T.B., private communication.

Figure Captions

Figure 1 CMA diagram for a one-component plasma. Axes are squares of normalized plasma frequency ($\alpha^2 \equiv \omega_p^2/\omega^2$) and electron cyclotron frequency ($\beta^2 \equiv \omega_c^2/\omega^2$). Numbered areas indicate various propagation regimes; the line R = ∞ represents the electron cyclotron resonance.

Figure 2 Absorption coefficient α vs. normalized frequency ω/ω_c for (a) fast mode, 11.3 keV; (b) fast mode, 45.1 keV; (c) slow mode, 11.3 keV; (d) slow mode, 45.1 keV. Gaps in the curve occur where the mode becomes evanescent.

Figure 3 The geometry of the heating zone (hatched) in toroidal and linear devices. In the first case magnetic field lines are perpendicular to the plane of the drawing, in the second case they are roughly parallel to the axis of the machine.

Figure 4 Axial magnetic field and potential profiles for TMX, MFTF-B and TASKA. Arrows indicate areas where ECRH is applied.

Figure 5 TASKA - magnetic field lines, resonance surfaces and ray trajectories with absorption profiles for a fast wave (O-mode) launched in different directions. Arrows represent the direction of wave vectors $\bar{k}$. Temperatures are (a) 5 keV; (b) 10 keV; (c) 30 keV; (d) 60 keV.

Figure 6 MFTF-B - ray trajectories and absorption profiles at 50 keV in the thermal barrier for (a) a slow wave and (b) a fast wave, and in the plug for (c) a slow wave and (d) a fast wave.

Figure 7 TMX - (a) resonance and cut-off surfaces and field lines in the yin-yang cell. (b) An enlarged section of (a), showing ray trajectories and absorption profiles. Electron temperature in 200 eV. Shaded areas are evanescent for the slow (X-) mode.

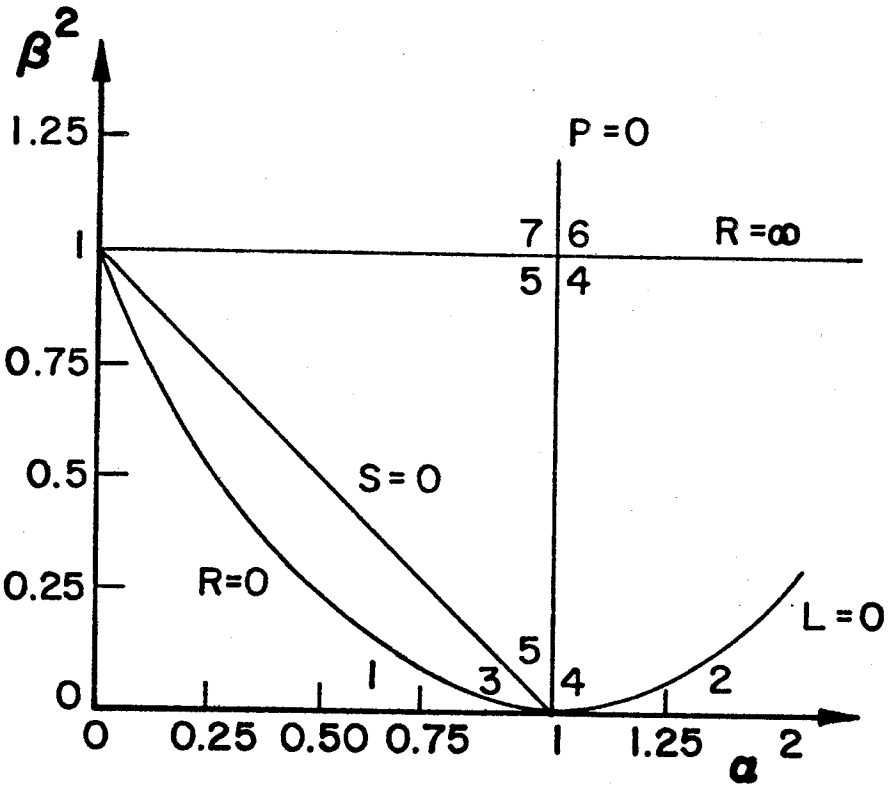

FIGURE 1

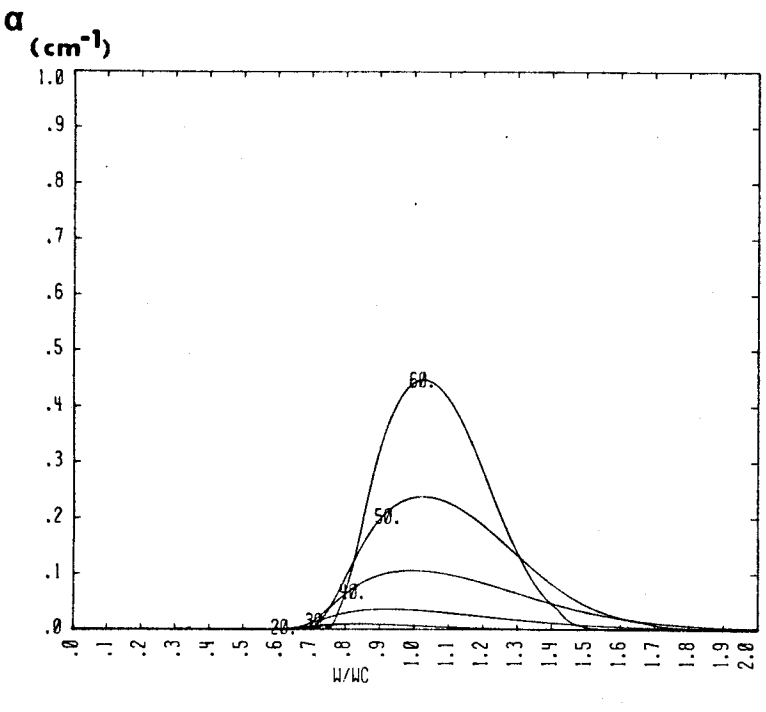

(a)

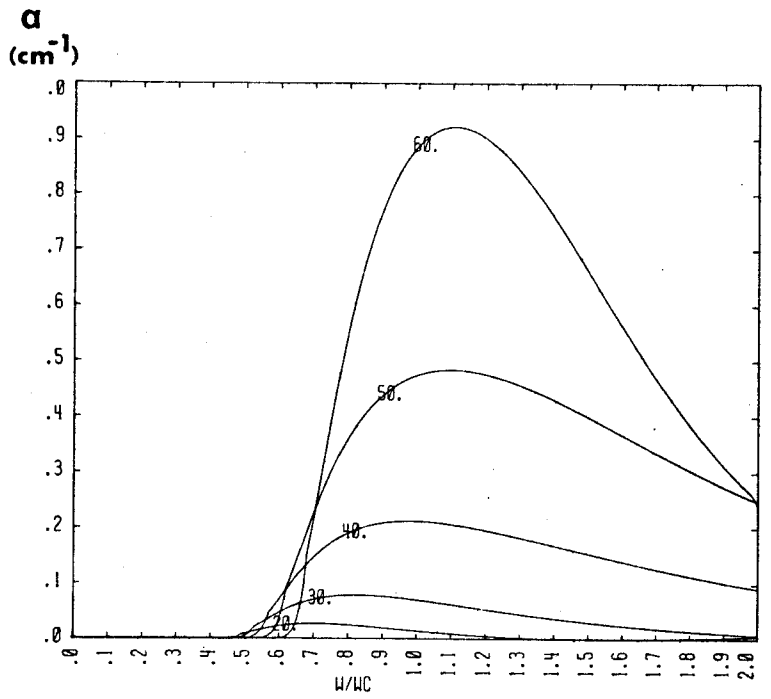

(b)

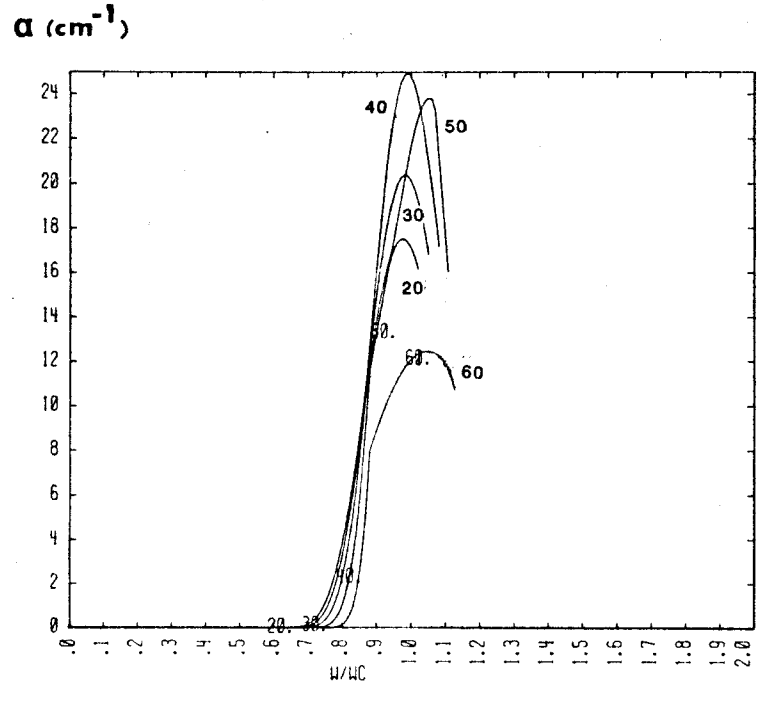

(c)

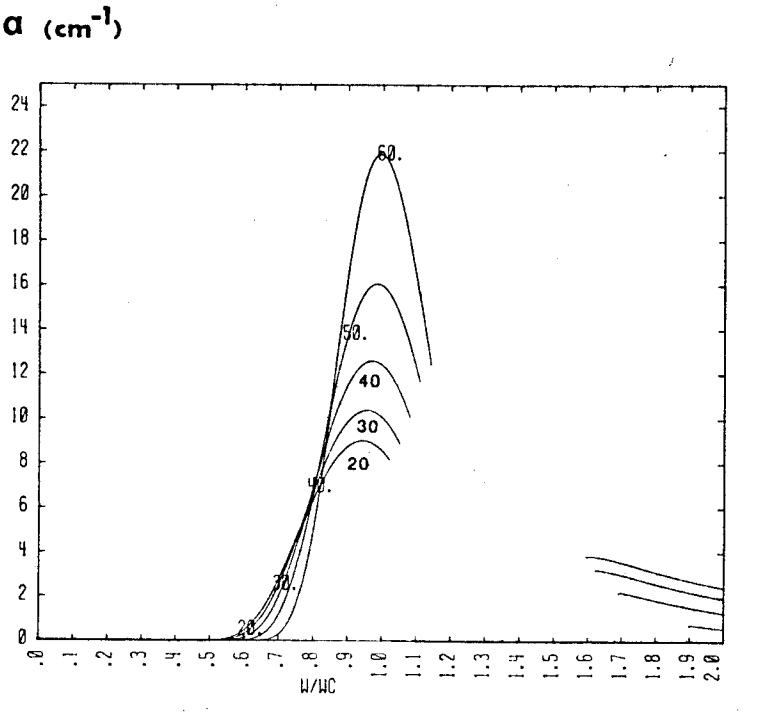

(d)

FIGURE 2

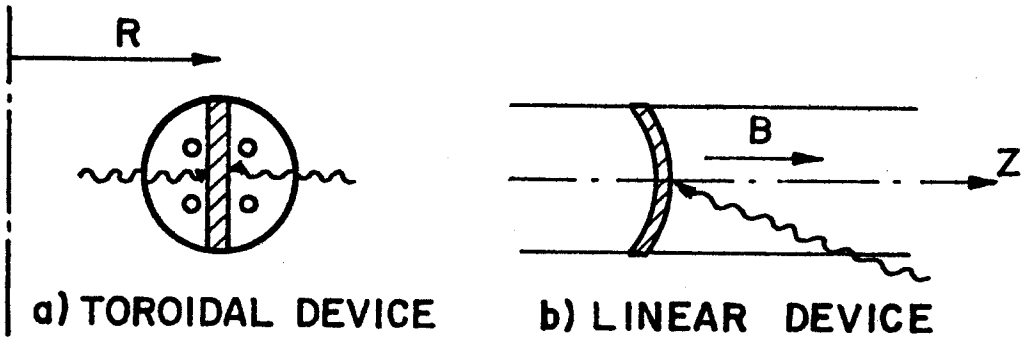

FIGURE 3

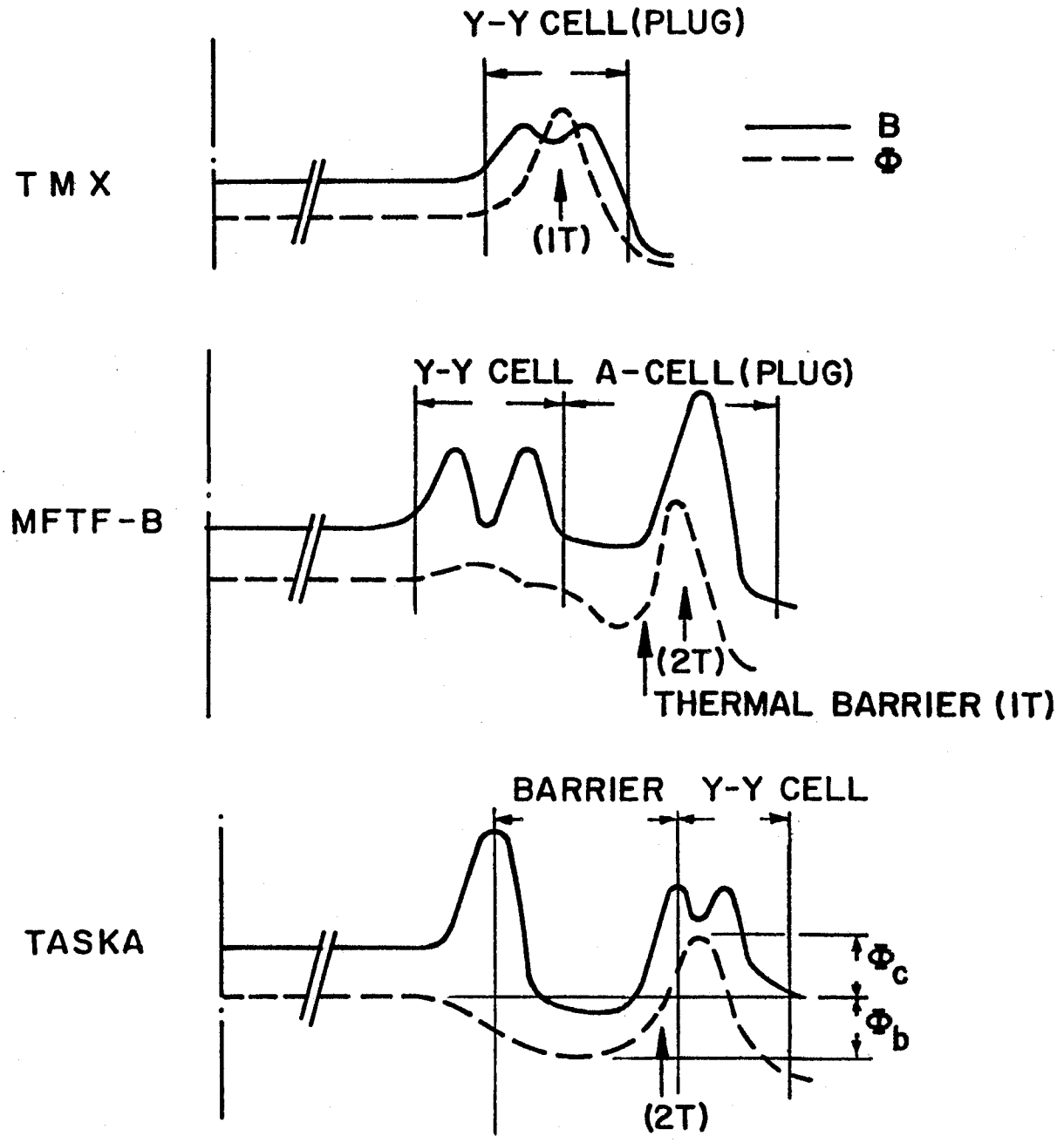
Y-Y CELL(PLUG)
TMX
B
Φ
(1T)
Y-Y CELL A-CELL(PLUG)
MFTF-B
(2T)
THERMAL BARRIER (1T)
BARRIER Y-Y CELL
TASKA
Φc
Φb
(2T)

FIG. 4

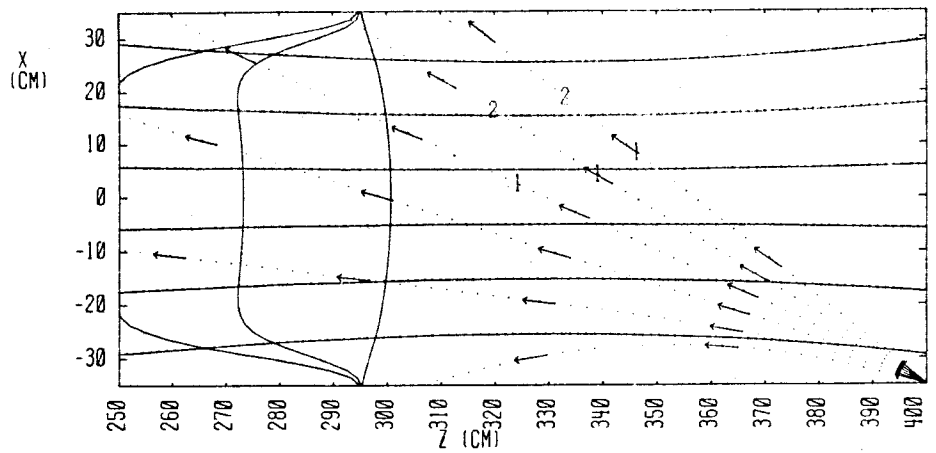

ORDINARY MODE
FREQUENCY 56. GHZ
B FIELD AT (0.0.300.0) 1.9925E+04 GAUSS
DENSITY AT (0.0.300.0) 1.0000E+13 1/CM**3
EL.TEMP AT (0.0.300.0) 5.00 KEV
INCIDENCE : FROM -75. TO -50. DEGREES (5.)

(a)

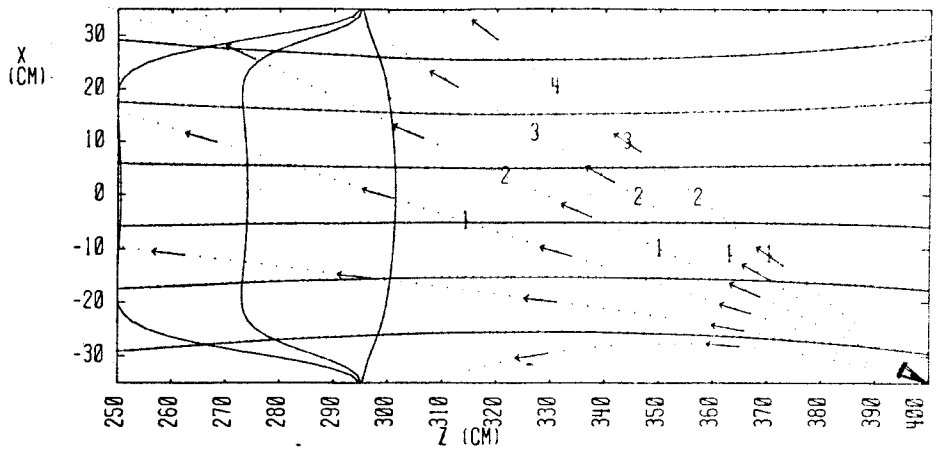

ORDINARY MODE
FREQUENCY 56. GHZ
B FIELD AT (0.0.300.0) 1.9849E+04 GAUSS
DENSITY AT (0.0.300.0) 1.0000E+13 1/CM**3
EL.TEMP AT (0.0.300.0) 10.00 KEV
INCIDENCE : FROM -75. TO -50. DEGREES (5.)

(b)

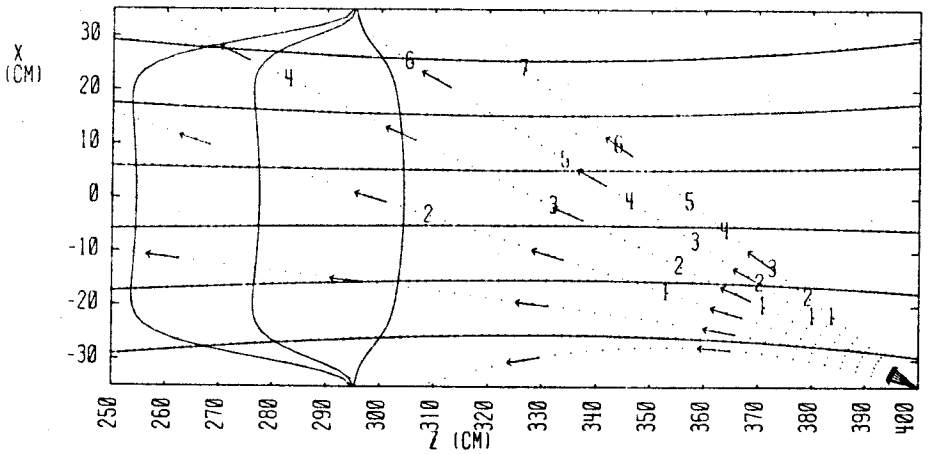

ORDINARY MODE
FREQUENCY 56. GHZ
B FIELD AT (0.0.300.0) 1.9545E+04 GAUSS
DENSITY AT (0.0.300.0) 1.0000E+13 1/CM**3
EL.TEMP AT (0.0.300.0) 30.00 KEV
INCIDENCE : FROM -75. TO -50. DEGREES (5.)

(c)

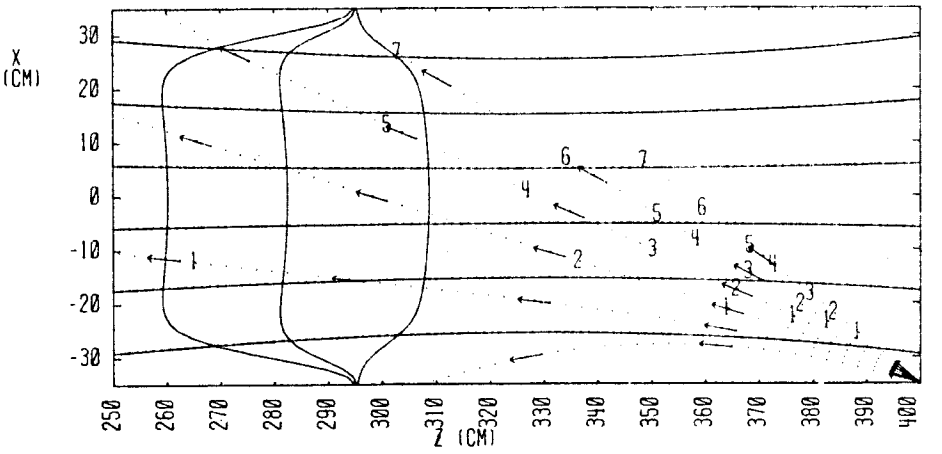

ORDINARY MODE
FREQUENCY 56. GHZ
B FIELD AT (0.0.300.0) 1.9079E+04 GAUSS
DENSITY AT (0.0.300.0) 1.0000E+13 1/CM**3
EL.TEMP AT (0.0.300.0) 60.00 KEV
INCIDENCE : FROM -75. TO -50. DEGREES (5.)

(d)

FIGURE 5

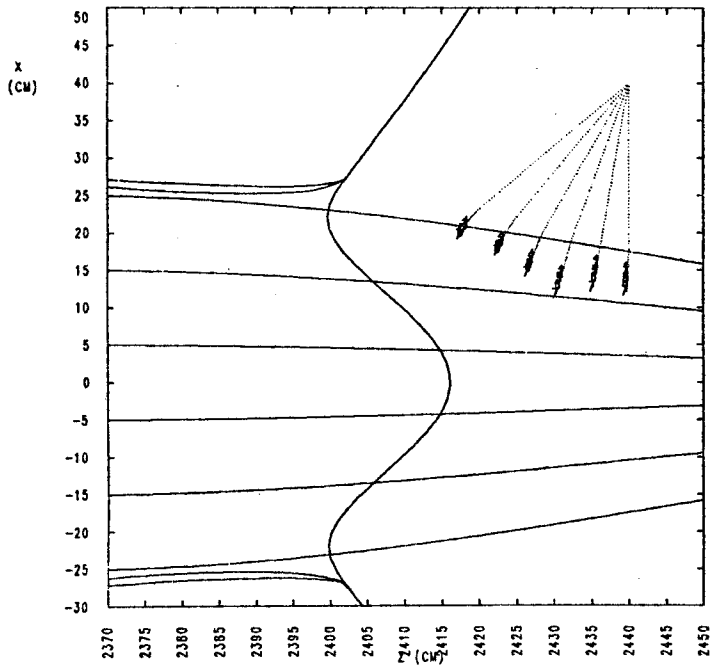

EXTRAORDINARY MODE
FREQUENCY 28. GHZ
B FIELD AT (0,0, 2370) 9.3240E+03 GAUSS
DENSITY AT (0,0, 2370) 6.5534E+12 1/CM**3
ELECTRON TEMPERATURE AT (0,0, 2370) 50.00 KEV
INCIDENCE : FROM -180. TO -130. DEGREES (10.)

(a)

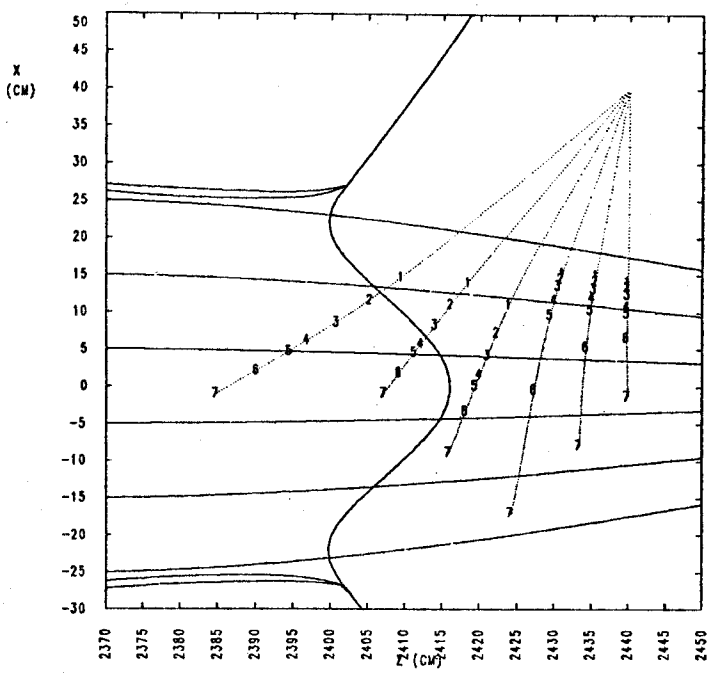

ORDINARY MODE
FREQUENCY 28. GHZ
B FIELD AT (0,0,2370) 9.3240E+03 GAUSS
DENSITY AT (0,0, 2370) 6.5534E+12 1/CM**3
ELECTRON TEMPERATURE AT (0,0,2370) 50.00 KEV
INCIDENCE : FROM -180. TO -130. DEGREES (10.)

(b)

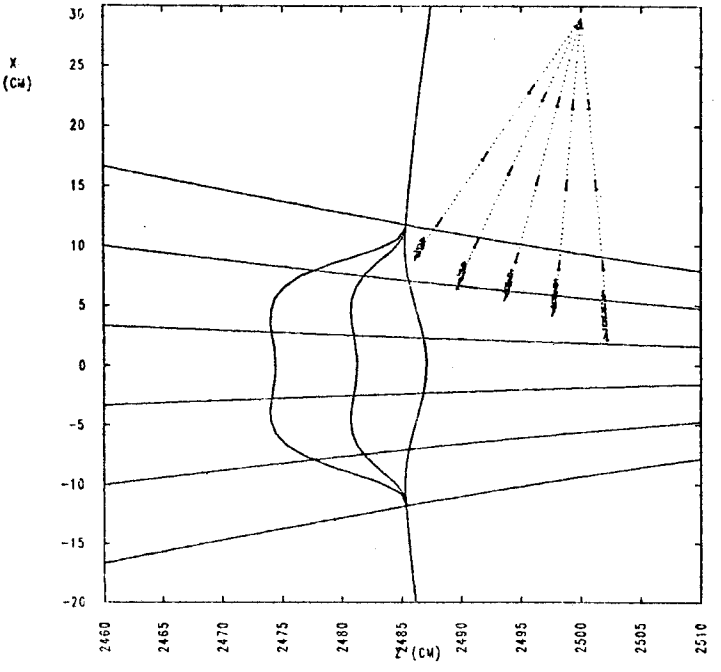

EXTRAORDINARY MODE
FREQUENCY 56. GHZ
B FIELD AT (0,0, 2460) 1.9419E+04 GAUSS
DENSITY AT (0,0, 2460) 5.5913E+12 1/CM**3
ELECTRON TEMPERATURE AT (0,0, 2460) 50.00 KEV
INCIDENCE : FROM -185. TO -145. DEGREES (10.)

(c)

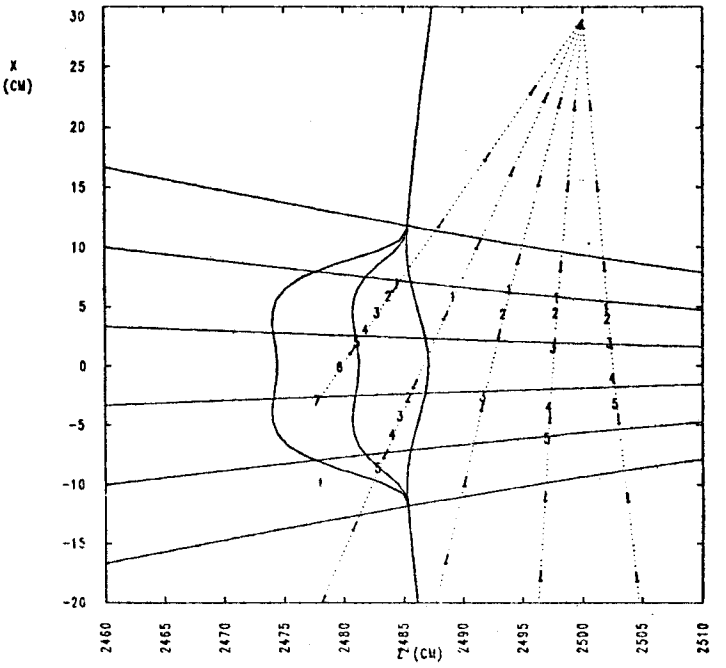

ORDINARY MODE
FREQUENCY 56. GHZ
B FIELD AT (0,0,2460) 1.9419E+04 GAUSS
DENSITY AT (0,0,2460) 5.5913E+12 1/CM**3
ELECTRON TEMPERATURE AT (0,0, 2460) 50.00 KEV
INCIDENCE : FROM -185. TO -145. DEGREES (10.)

(d)

FIGURE 6

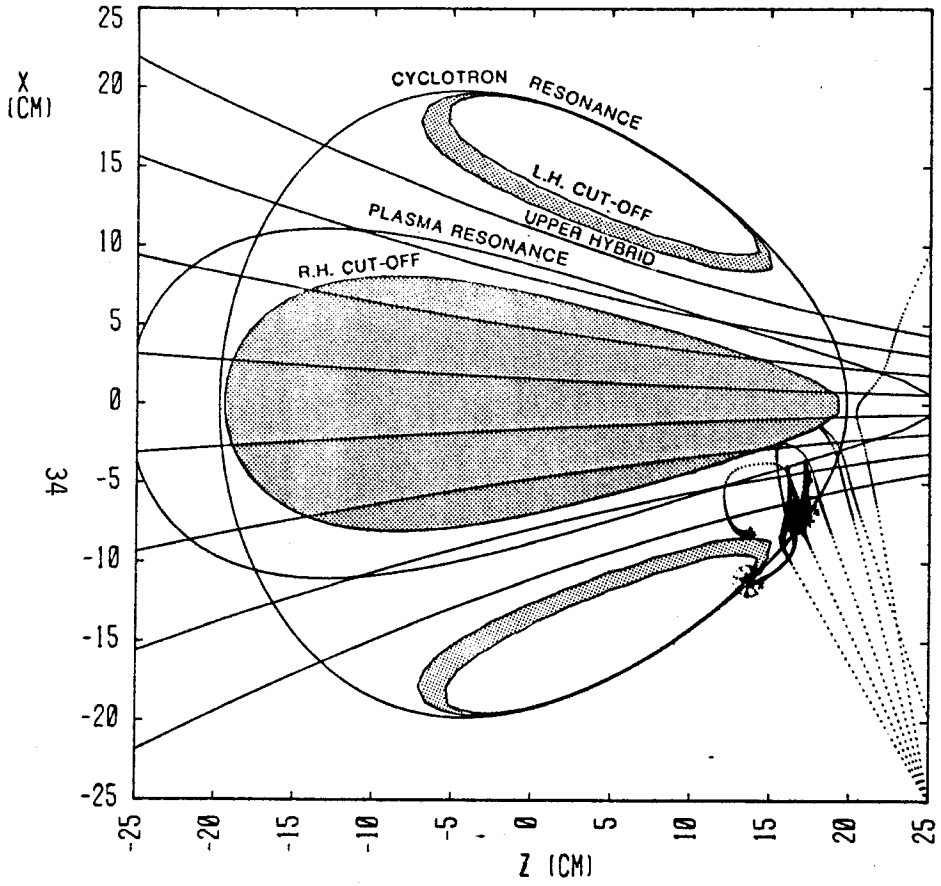

EXTRAORDINARY MODE
FREQUENCY 28. GHZ
B FIELD AT (0.0, 0.0) 8.5000E+03 GAUSS
DENSITY AT (0.0, 0.0) 5.0000E+13 1/CM**3
EL.TEMP AT (0.0, 0.0) 0.20 KEV
INCIDENCE : FROM -30. TO -10. DEGREES (5.)

(a)

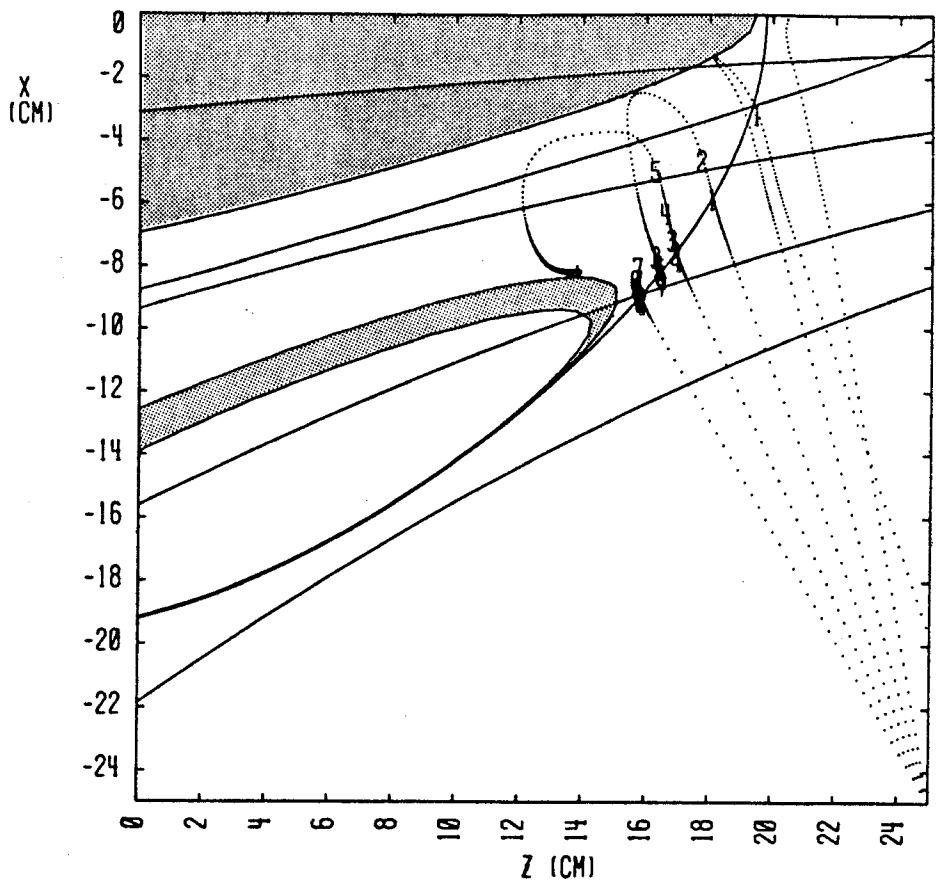

EXTRAORDINARY MODE
FREQUENCY 28. GHZ
B FIELD AT (0.0, 0.0) 8.5000E+03 GAUSS
DENSITY AT (0.0, 0.0) 5.0000E+13 1/CM**3
EL.TEMP AT (0.0, 0.0) 0.20 KEV
INCIDENCE : FROM -30. TO -10. DEGREES (5.)

(b)

FIGURE 7